Satellite Detection and Nowcasting High-altitude Ice Crystals

YL NG*, HF LAW, JCW LEE, KK HON, LO LI and PW LI
Hong Kong Observatory
134A, Nathan Road, Kowloon, Hong Kong

October 3, 2017

1 Introduction

Over the last 20 years, the aviation industry has documented more than 100 incidents in which turbofans have lost power during high-altitude flights, and HAIC are believed to have caused most or all of these events [1]. The phenomenon has become more common as engine manufacturers introduce higher-bypass turbofans and airlines fly at higher altitudes. When an aircraft flies through regions of high ice water content, ice crystals may damage the blades, or they could be ingested by the turbofans and melted on warm engine surfaces. The resulting thin film of water attracts more ice crystals and significant icing could cause a temporary loss of engine power.

In general, regions of HIWC are related to deep convection. Strong updraft in deep convective clouds can carry water droplets to high altitude rapidly. These water droplets then freeze to small crystals, which can be as small as 40 µm. As these ice crystals are small, they cannot be detected by on-board weather radar and could possibly be a threat to aviation.

In this study, we aim to use satellite data to mark regions of HAIC in areas of deep convection. We first used the brightness temperature difference between a water vapour channel (9.6 µm) and an infrared channel (10.4 µm) to identify overshooting tops. Then other infrared channels, which have different absorption coefficients for ice and water, were included to locate regions with ice particles. We performed random forest analysis to data from Himawari-8 for identifying HAIC. It can be used to rank the importance of variables and is useful for eliminating uninformative satellite channels.

A simplified method was derived from the final random forests model and only required the calculation of split windows with imposed cut-off criteria. The criteria were chosen with reference to the random forest decision trees and meteorological conceptual models. The method is very easy to implement and has demonstrated a comparable skill to other methods in [2].

2 Methodology

Based on the importance of channels identified through random forest analysis and the physical properties of ice, a total of five channels were chosen: $B3_{0.64\ \mu m}$, $B7_{3.9\ \mu m}$, $B9_{6.9\ \mu m}$, $B12_{9.6\ \mu m}$ and $B13_{10.4\ \mu m}$. Visible channel

($B3_{0.64\ \mu m}$) was ranked quite high in its usefulness because it has a higher resolution and the solar reflectivity of ice and water is distinctive. EUMETSAT Severe Storm RGB [3] used split window $B7_{3.9\ \mu m}$ and $B13_{10.4\ \mu m}$ for their green channel to identify very cold cloud tops with strong updraft (high $B7_{3.9\ \mu m}$ reflectivity by small ice particles). $B9_{6.9\ \mu m}$ is a water vapour (WV) channel, which was commonly used with $B13_{10.4\ \mu m}$ to locate overshooting tops. The ozone channel ($B12_{9.6\ \mu m}$) could differentiate cold (polar) and warm (mid-level, subtropical) air masses based on ozone concentration differences. Location of the tropopause could influence convective clouds and the height of which the ice particles might reach.

Kwon et al. showed improvements in detecting deep convective cloud heights by using ozone channel 9.7 μm [4]. They noted that $B12_{9.6\ \mu m}$–$B13_{12.4\ \mu m}$ can be a better indicator for the deep convective activity than $B9_{6.9\ \mu m}$–$B13_{10.4\ \mu m}$. With higher cloud tops, the absorption effects by H_2O get smaller and thus $B9_{6.9\ \mu m}$–$B13_{10.4\ \mu m}$ approaches zero. Whereas $B12_{9.6\ \mu m}$ shows significantly higher values than other channels due to the warming by stratospheric ozone, which results in the sharply increasing values of $B12_{9.6\ \mu m}$–$B13_{10.4\ \mu m}$. From our random forests, the high importance of $B12_{9.6\ \mu m}$–$B13_{10.4\ \mu m}$ is in accordance with this theory.

Split windows	Cut-off points (K)	Properties
$B1_{0.47\ \mu m}$, $B2_{0.51\ \mu m}$, $B3_{0.64\ \mu m}$	> 0.4	daytime
$B7_{3.9\ \mu m} - B13_{10.4\ \mu m}$	> 50	small ice particles for very cold cloud tops (given daytime)
$B9_{6.9\ \mu m}$–$B13_{10.4\ \mu m}$	> -1.5	deep convective activity of clouds
$B12_{9.6\ \mu m}$–$B13_{10.4\ \mu m}$	> 6.5 and < 19	deep convective activity of high clouds

Table 1: Split windows algorithm (given $B13_{10.4\ \mu m} < 243$ K) with corresponding cut-off points.

3 Results

Blue polygons indicating deep convective activity of high clouds are plotted on each satellite picture, which is updated every 10 minutes. If there are sufficient solar radiation, yellow polygons are also given in the satellite picture for small ice particles for very cold cloud tops. Atmospheric motion vectors are derived by comparing two consecutive satellite pictures and they would then be used to estimate the 1 hour forecast positions.

Red dot showed the location of an icing event with moderate severity reported by pilot at 0345Z and FL250.

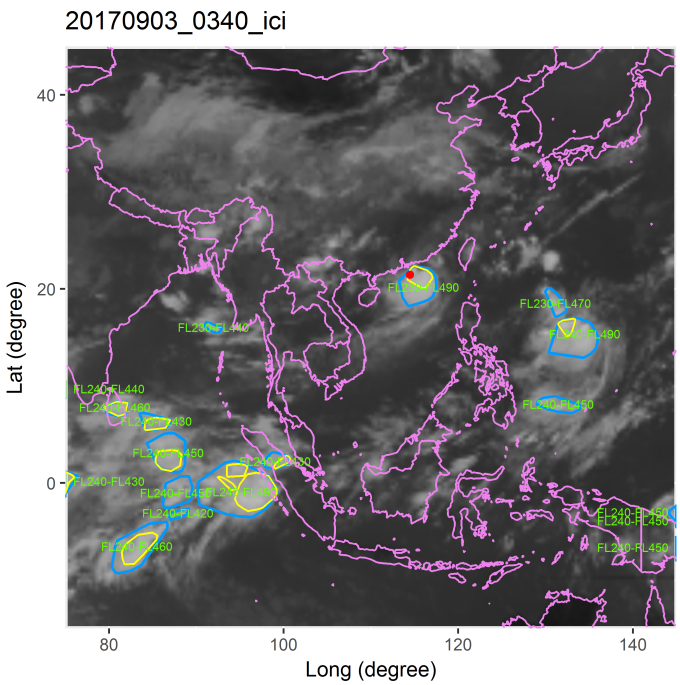

Deep convection for high clouds
$19 > \mathrm{B12}_{9.6\ \mu m} - \mathrm{B13}_{10.4\ \mu m} > 6.5$ in blue;

Small ice particles for very cold cloud tops
$\mathrm{B7}_{3.9\ \mu m} - \mathrm{B13}_{10.4\ \mu m} > 50$ in yellow.

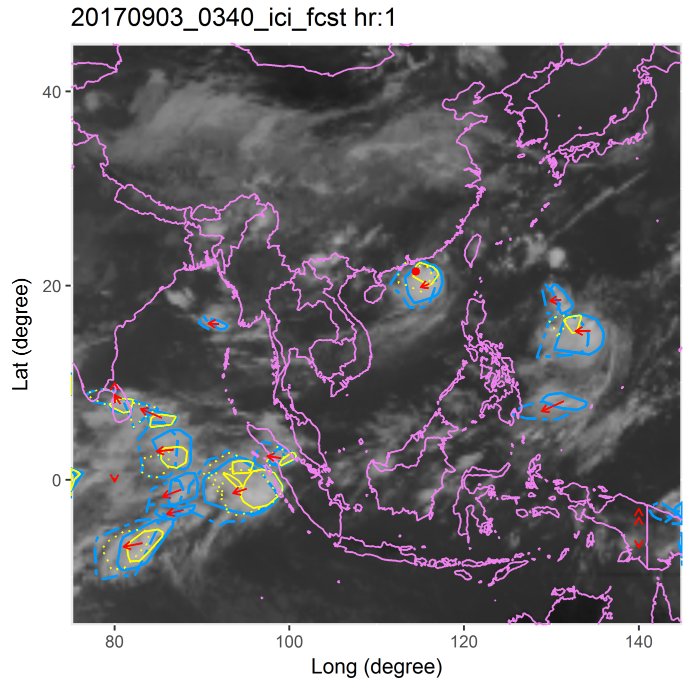

Polygons with dotted lines show 1 hour forecast positions estimated using atmospheric motion vectors (red arrows) derived from Satellite pictures on 3 September 2017 at 0330Z and 0340Z.

Longer-term forecast will be done by applying the algorithm to model-simulated satellite channels. An example is shown:

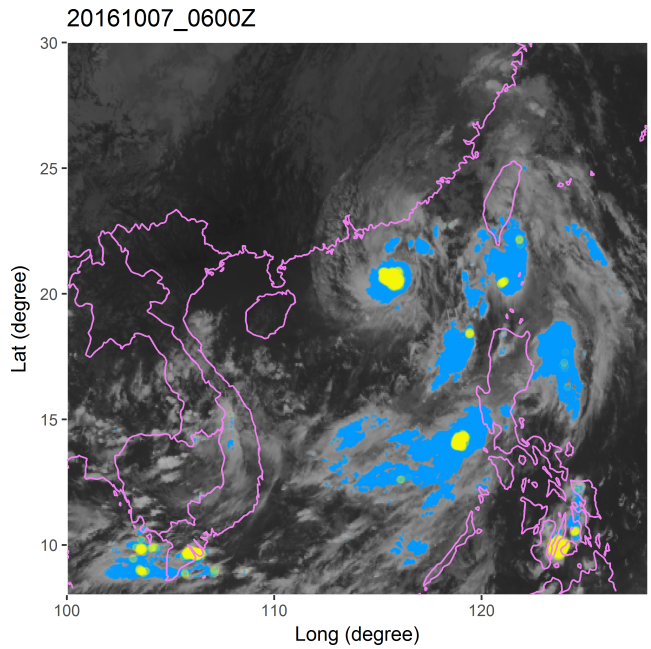

Deep convection for high clouds
$19 > B12_{9.6\ \mu m} - B13_{10.4\ \mu m} > 6.5$ in blue;

Small ice particles for very cold cloud tops
$B7_{3.9\ \mu m} - B13_{10.4\ \mu m} > 50$ in yellow.

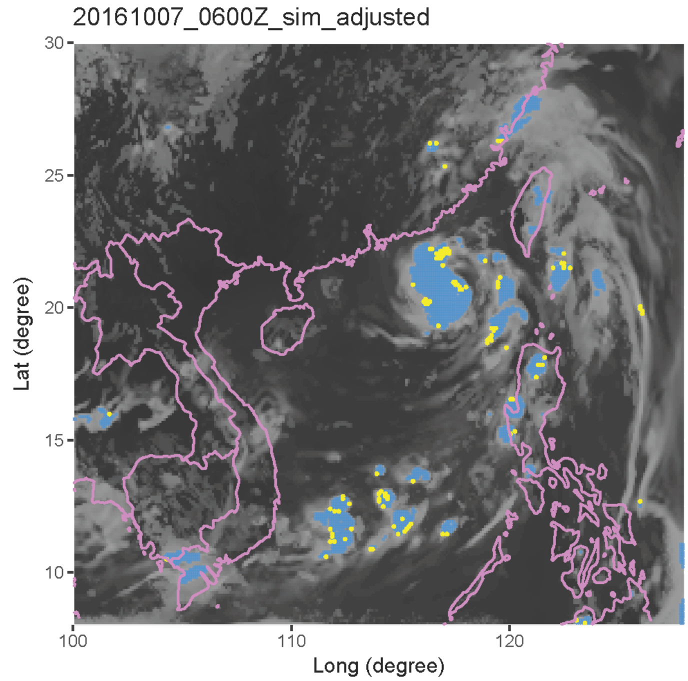

Model run on 7 October 2016 at 0000Z, forecast hour: +6 hours. Simulated satellite channels have been adjusted using histogram matching method for observed and simulated pictures at 0000Z.

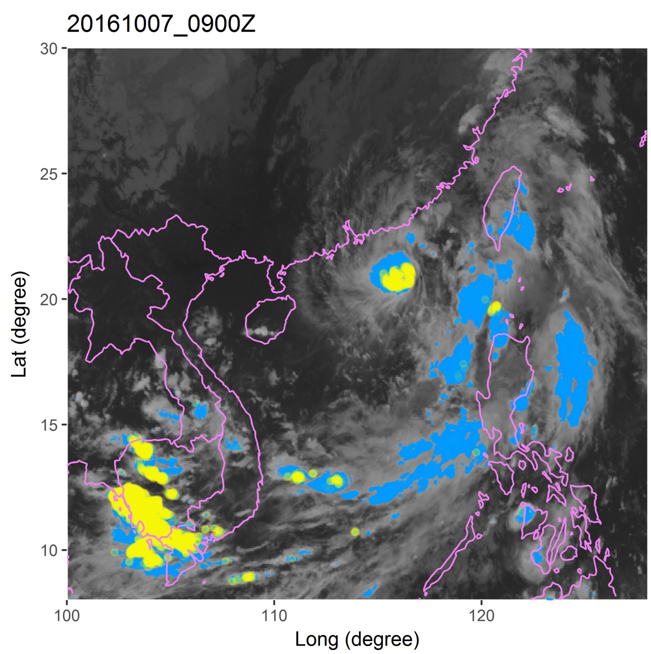

Deep convection for high clouds
$19 > B12_{9.6\ \mu m} - B13_{10.4\ \mu m} > 6.5$ in blue;

Small ice particles for very cold cloud tops
$B7_{3.9\ \mu m} - B13_{10.4\ \mu m} > 50$ in yellow.

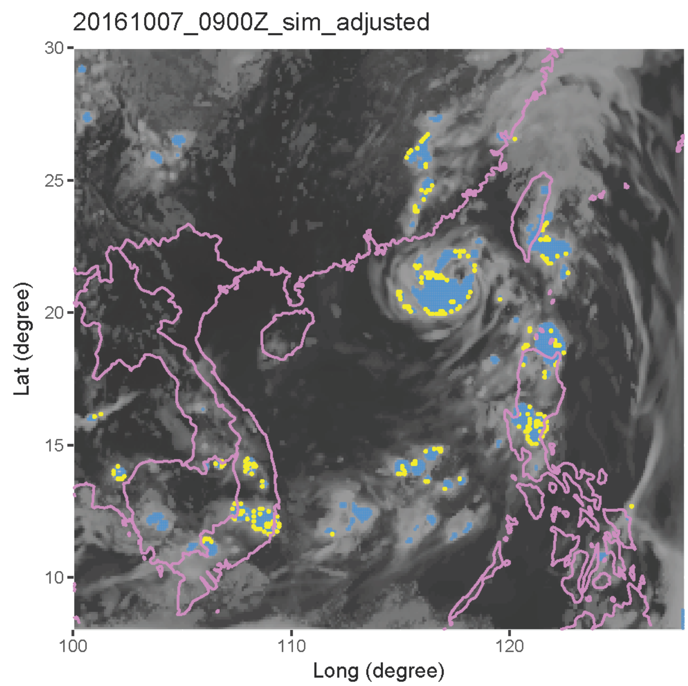

Model run on 7 October 2016 at 0000Z, forecast hour: +9 hours. Simulated satellite channels have been adjusted using histogram matching method for observed and simulated pictures at 0000Z.

4 Discussion

Algorithm	***POD***	***FAR***	True skill statistics
Himawari-8	0.55	0.13	**0.42**
CIP (NCAR)	0.76	0.33	**0.43**
SIGMA (Meteo-France)	0.59	0.26	0.33
GDCP (NASA)	0.76	0.67	0.09

Table 2: CIP, SIGMA, and GDCP for AIRSII research aircraft evaluation.

The split windows algorithm demonstrated here using Himawari-8 cases have skill that is comparable with NCAR's *Current Icing Product* (CIP), Meteo-France's *System of Icing Geographic identification in Meteorology for Aviation* (SIGMA) and NASA's *GOES-derived Cloud Products* (GDCP) [2].

The algorithm was derived based on a total of 14 icing cases reported by pilot, which were justified with the measured static air temperature anomalies, between April 2015 and October 2016. Its performance was shown be comparable with other algorithms. However, POD was not outstanding. Fine tuning of the algorithm could be made possible if there were more cases to be included. Moreover, forecasting with simulated satellite channels had been explored and the results seemed to be promising. Further investigation and verification will be carried out in future studies.

References

[1] J. Mason, Engine power loss in ice crystal conditions, *Aero* QTR4 (2007).

[2] M. Chapman, A. Holmes and C. Wolff, Verification of aviation icing algorithms from the second alliance icing research study, 12th Conference on Aviation Range and Aerospace Meteorology, https://ams.confex.com/ams/Annual2006/techprogram/paper_104158.htm (accessed Sep. 15 2016).

[3] J. Kerkmann, Understanding convective clouds through the eyes of (MGS) Cloud Particle Size, http://www.rtc.mgm.gov.tr/FILES/KURS/334/DOCS/JochenKerkman3.pdf

[4] Kwon, EH., Sohn, BJ., Schmetz, J. et al. Asia-Pacific J Atmos Sci (2010) 46: 11. doi:10.1007/s13143-010-0002-7